UC Berkeley
UC Berkeley Previously Published Works

Title

Frontotemporal dementia with the V337M MAPT mutation

Permalink

Journal

ISSN

Authors

Spina, Salvatore
Schonhaut, Daniel R
Boeve, Bradley F
et al.

Publication Date

DOI

Peer reviewed

Frontotemporal dementia with the V337M *MAPT* mutation
Tau-PET and pathology correlations

Salvatore Spina, MD, PhD
Daniel R. Schonhaut, BA
Bradley F. Boeve, MD
William W. Seeley, MD
Rik Ossenkoppele, PhD
James P. O'Neil, PhD
Andreas Lazaris, BA
Howard J. Rosen, MD
Adam L. Boxer, MD, PhD
David C. Perry, MD
Bruce L. Miller, MD
Dennis W. Dickson, MD
Joseph E. Parisi, MD
William J. Jagust, MD
Melissa E. Murray, PhD
Gil D. Rabinovici, MD

Correspondence to
Dr. Spina:
Salvatore.Spina@ucsf.edu

ABSTRACT

Objective: To assess the efficacy of [18F]AV1451 PET in visualizing tau pathology in vivo in a patient with frontotemporal dementia (FTD) associated with the V337M microtubule-associated protein tau (*MAPT)* mutation.

Methods: *MAPT* mutations are associated with the deposition of hyperphosphorylated tau protein in neurons and glia. The PET tracer [18F]AV1451 binds with high affinity to paired helical filaments tau that comprises neurofibrillary tangles in Alzheimer disease (AD), while postmortem studies suggest lower or absent binding to the tau filaments of the majority of non-AD tauopathies. We describe clinical, structural MRI, and [18F]AV1451 PET findings in a V337M *MAPT* mutation carrier affected by FTD and pathologic findings in his affected mother and in an unrelated V337M *MAPT* carrier also affected with FTD. The biochemical similarity between paired helical filament tau in AD and *MAPT* V337M predicts that the tau pathology associated with this mutation constitutes a compelling target for [18F]AV1451 imaging.

Results: We found a strong association between topography and degree of [18F]AV1451 tracer retention in the proband and distribution of tau pathology in the brain of the proband's mother and the unrelated V337M mutation carrier. We also found a significant correlation between the degree of regional MRI brain atrophy and the extent of [18F]AV1451 binding in the proband and a strong association between the proband's clinical presentation and the extent of regional brain atrophy and tau accumulation as assessed by structural brain MRI and [18F]AV1451PET.

Conclusion: Our study supports the usefulness of [18F]AV1451 to characterize tau pathology in at least a subset of pathogenic *MAPT* mutations. ***Neurology® 2017;88:758-766***

GLOSSARY

Aβ = β-amyloid; **AD** = Alzheimer disease; **bvFTD** = behavioral variant frontotemporal dementia; **4R** = 4-repeat; **FTD** = frontotemporal dementia; **FTLD** = frontotemporal lobar degeneration; **MAPT** = microtubule-associated protein tau; **NFT** = neurofibrillary tangle; **PHF** = paired helical filaments; **ROI** = region of interest; **SUVr** = standardized uptake value ratio; **TDP-43** = TAR DNA binding protein–43 kDa; **3R** = 3-repeat; **UCSF** = University of California San Francisco; **VBM** = voxel-based morphometry.

Frontotemporal dementia (FTD) is the second most prevalent type of dementia before age 65.[1–4] Mutations in the microtubule-associated protein tau (*MAPT*) gene were the first to be associated with inherited FTD and to cause deposition of hyperphosphorylated tau protein in either neurons or both neuronal and glial cells.[5–9] The V337M *MAPT* mutation has been associated with FTD with prominent antisocial behavior and paranoia and severe frontotemporal and limbic degeneration.[7,10,11] At autopsy, abundant neuronal tau deposits composed of paired helical filaments (PHF) tau made up of a mix of hyperphosphorylated tau protein with 3-repeat (3R) and 4-repeat (4R) microtubule-binding motifs are found. The conformation and biochemical composition of tau aggregates associated with this mutation are similar to those found in neurofibrillary tangles (NFTs) in Alzheimer disease (AD), with electron

microscopy confirming the presence of PHF,[11,12] although there are differences between the 2 disorders in regard to extent, laminar distribution, and regional involvement of the aggregates.[11,12]

The PET tracer [18F]AV1451 selectively binds to NFTs over β-amyloid (Aβ) plaques in postmortem tissue samples with AD neuropathology.[13,14] Early human in vivo studies in AD are compatible with Braak staging and the expected distribution of tau pathology.[15–17] While [18F]AV1451 binds with high affinity to PHF tau that comprises NFT in AD, postmortem studies suggest lower affinity or absent binding to the other types of tau filaments found in the majority of non-AD tauopathies.[14,18–20] We describe clinical, structural MRI, and [18F]AV1451 PET findings in a V337M *MAPT* mutation carrier with behavioral variant FTD (bvFTD), as well as pathologic findings in his affected mother and in an unrelated patient with bvFTD who carried the same *MAPT* mutation.

METHODS Patients. *Family A.* Proband (patient A.IV.1). A 30-year-old right-handed man developed compulsions, irritability, and mental inflexibility. Later, he developed difficulties with memory, completion of tasks, and orientation. He became impulsive, disinhibited, and unempathetic. He developed paranoid ideations and inappropriate behavior toward colleagues that resulted in criminal charges. By age 58, his speech output and ability to follow a conversation declined. He became progressively apathetic and increasingly adherent to a strict daily routine. Genetic testing revealed a V337M *MAPT* mutation in the proband and affected family members.

Family history. The proband's maternal great grandparent (patient A.I.1) and a maternal grandparent (patient A.II.1) died of dementia with behavioral abnormalities. The proband's mother (patient A.III.1) became disinhibited in her 40s and functionally impaired by age 50. She exhibited a slow decline in cognition with ritualistic behavior, mental rigidity, and restricted food choices. She died at age 82. Her sibling developed personality changes at age 50 and died at age 64. The proband's sibling developed behavioral changes in their late 30s (figure 1).

Family B. Patient B.II.1. At age 55, this right-handed woman lost interest in her business. She became irritable, verbally abusive, and emotionally blunted. At age 57, she began using complex circumlocutions to compensate for loss of vocabulary. She became mentally rigid and struggled to recognize faces. At age 60, she lost interest in personal hygiene. She began eating the same type of food and gained 20 pounds in 1 year. Her neurologic examination at age 63 revealed surface dyslexia, phonemic paraphasia, mild dysarthria, and postural tremor. Neuropsychological testing revealed marked impairment in memory, executive function, and semantic knowledge. Her brain MRI showed symmetrical frontotemporal atrophy. She was diagnosed with bvFTD. She died at age 68. The V337M *MAPT* mutation was identified in the patient and affected family members.

Family history. The family history was notable for her father (patient B.I.1) developing FTD at age 61 and dying at age 66 of myocardial infarct. An autopsy revealed frontotemporal lobar degeneration (FTLD). Her father's 4 siblings had a similar illness with onset in their 40s or 50s. Her mother died of suicide at age 43. The patient's sister was diagnosed with schizoaffective disorder in early life and later developed early-onset dementia (figure 1).

Controls. For the neuroimaging studies, 20 cognitively normal, right-handed men were recruited from studies of normal aging at University of California San Francisco (UCSF) (mean age 65.8 ± 5.2 years, education 15.7 ± 1.3 years).[21] Controls performed normally on neuropsychological testing, had no significant history of neurologic illness, and were determined to be cognitively normal by consensus diagnosis.

MRI acquisition and processing and voxel-based morphometry. Patient A.IV.1 and all controls were scanned at the UCSF Neuroimaging Center on a Siemens 3T Tim Trio MRI unit. T1-weighted magnetization-prepared rapid gradient echo sequences were collected using previously described acquisition parameters.[22] MRIs were processed with FreeSurfer 5.1, and cortical regions of interest (ROIs) and thickness measurements were obtained in native space.[23,24] Voxel-based morphometry (VBM) comparing the proband to a healthy control group with Statistical Parametric Mapping 12 (SPM12) software was implemented in Matlab 8.3 (see appendix e-1 at Neurology.org).

PET acquisition and processing. Patient A.IV.1 underwent PET imaging with [18F]AV1451 at Lawrence Berkeley National Laboratory on a Siemens Biograph Truepoint 6 scanner in 3-dimensional acquisition mode. The PET radioligand was synthesized at the Lawrence Berkeley National Laboratory's Biomedical Isotope Facility, and 100 minutes of dynamic data were recorded immediately after 9.5-mCi intravenous injection of [18F]AV1451 and 120 to 150 minutes after injection. PET data were reconstructed as previously described.[16,25] PET frames were

Figure 1 Pedigree of family A and family B
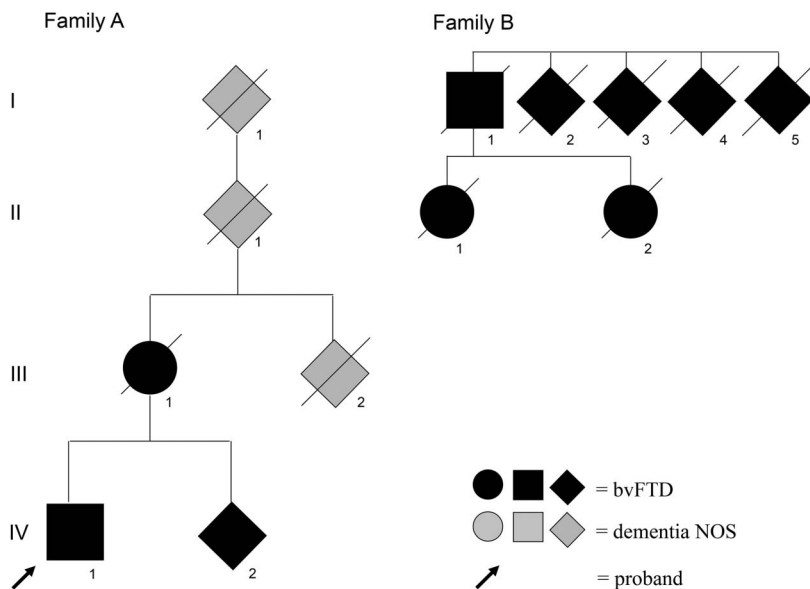
bvFTD = behavioral variant frontotemporal dementia; NOS = not otherwise specified.

realigned for motion correction and coregistered to the patient's T1-weighted MRI acquired within 1 week of the PET scan. A standardized uptake value ratio (SUVr) image was created from the 80- to 100-minute postinjection PET data with FreeSurfer-defined cerebellar gray matter used as a reference region.[15] We recently demonstrated that, despite slow tracer pharmacokinetics, 80- to 100-minute SUVr values are a reasonable method to quantify [^{18}F]AV1451 retention in cross-sectional studies.[26]

ROI analysis. Mean [^{18}F]AV1451 SUVr values and cortical thickness measurements were acquired in 68 left and right hemisphere FreeSurfer-defined cortical regions. For each region, a Z score was calculated representing the patient's cortical thickness relative to that of the 20 controls. The Spearman correlation coefficient was used to test the relationship between cortical thickness Z scores and [^{18}F]AV1451 SUVr means across the same regions.

CSF Aβ/tau profile screening. CSF concentrations of Aβ$_{1-42}$, total tau protein, and phosphorylated tau protein were assessed in patient A.IV.1 at the University of Pennsylvania Biomarker Research Laboratory as previously described.[27]

Neuropathology. The brain of the mother of patient A.IV.1 was evaluated at Mayo Clinic Rochester and Jacksonville according to the Consortium to Establish a Registry for Alzheimer's Disease protocol.[28] The brain autopsy of patient B.II.1 was performed at UCSF. Immunohistochemistry against phosphorylated tau, Aβ, α-synuclein, and TAR DNA binding protein–43 kDa (TDP-43) was carried out (appendix e-1). 3R and 4R tau immunohistochemistry was carried on the brain of patient B.II.1. AD neuropathology was assessed with the National Institute of Aging and Alzheimer's Association criteria.[29] FTLD neuropathology, TDP-43 subtype, and hippocampal sclerosis were assessed as previously described.[30,31] All pathologic assessments were performed by investigators blinded to [^{18}F]AV1451PET results.

Standard protocol approvals, registrations, and patient consents. All elements of the study were approved by the Institutional Review boards at UCSF, Mayo Clinic, and Lawrence Berkeley National Laboratory. Informed consent was provided by all controls and by the patient's surrogate decision maker.

RESULTS **Clinical evaluation.** Neurologic examination of patient A.IV.1 showed flat affect and diminished attention. His speech was fluent and grammatically intact with no word finding difficulties. Surface dyslexia and semantic paraphasias were noted. Extraocular movements were intact. There was mild hypomimia. Mild resting and postural tremor was noted in the upper extremities. Bilateral palmomental reflex was seen. Deep tendon reflexes, cerebellar testing, and gait were unremarkable. Neuropsychological assessment revealed Mini-Mental State Examination score of 20/30, prominent executive dysfunction, impaired response inhibition and tendency to perseveration, markedly impaired semantic knowledge and affect recognition, and marked verbal memory deficits (table e-1). He was diagnosed with bvFTD.[3]

CSF Aβ/tau profile screening. CSF analysis for patient A.IV.1 revealed normal Aβ$_{1-42}$ (290 pg/mL, normal >250 pg/mL) and total tau protein (30 pg/mL, normal <93 pg/mL) concentrations. Phosphorylated tau protein concentration was elevated (30 pg/mL, normal <23 pg/mL). Both total tau protein/Aβ$_{1-42}$ and phosphorylated tau/Aβ$_{1-42}$ ratios were normal (0.12 [normal <0.39] and 0.1 [normal <0.1], respectively).[27]

MRI results. The brain MRI of patient A.IV.1 (figure 2) displayed severe bilateral atrophy of the temporal poles, medial temporal lobes, orbitofrontal gyri (medial > lateral), anterior insulae, frontal poles, anterior cingulate gyri, and mesial portions of the superior frontal gyrus. To a lesser extent, there was also atrophy of the dorsolateral prefrontal gyri, as well as the middle and inferior temporal gyri. The perirolandic gyri and parietal and occipital lobes were much better preserved. There was marked atrophy of the amygdale and of the head of the caudate nuclei.

VBM revealed a significant pattern of cortical gray matter loss in the proband compared to controls in the bilateral anterior temporal lobes, anterior insulae, and orbitofrontal and anterior cingulate gyri ($p <$ 0.01 uncorrected, table e-2) (figure 2). FreeSurfer-based estimation of cortical thickness changes in the proband compared to the control showed a topographic pattern of atrophy similar to that measured by VBM (table e-2).

Tau-PET data. Visual inspection of the [^{18}F]AV1451 PET scan of patient A.IV.1 showed areas of highest tracer binding in the bilateral frontal pole, medial orbitofrontal cortex, inferior temporal lobe, insular cortex, anterior cingulate, dorsolateral prefrontal cortex, and lateral temporal cortex (figure 2). [^{18}F]AV1451 time-activity curves from the frontal cortex vs the cerebellar gray matter reference regions are shown in figure e-1. The hippocampal formations were notably spared, while the entorhinal cortices and parahippocampal gyri showed intermediate levels of uptake. Extensive tracer uptake was also noted in the striata (particularly in their ventral portion) and globus pallidi, as well as in the lateral thalami and substantia nigra, although caution is warranted in the interpretation of these results because "off-target" binding unrelated to tau is seen in the same regions in normal controls.[14,17] Normalized tracer uptake levels (SUVr) for each ROI are reported in table e-2. Pearson correlation across the 68 FreeSurfer-defined cortical ROIs showed a strong correlation between regional gray matter volume and [^{18}F]AV1451 SUVr ($ρ = -0.54$, $p < 0.00001$) (figure 3). The Pearson correlation across the 68 FreeSurfer-defined cortical ROIs also showed a strong correlation between regional cortical thickness and [^{18}F]AV1451 SUVr ($ρ = -0.41$, $p < 0.001$).

Neuropathologic examination. *Patient A.III.1.* Severe atrophy was seen in the frontal and temporal lobes (figure 4, A and B), CA1 sector, and subiculum.
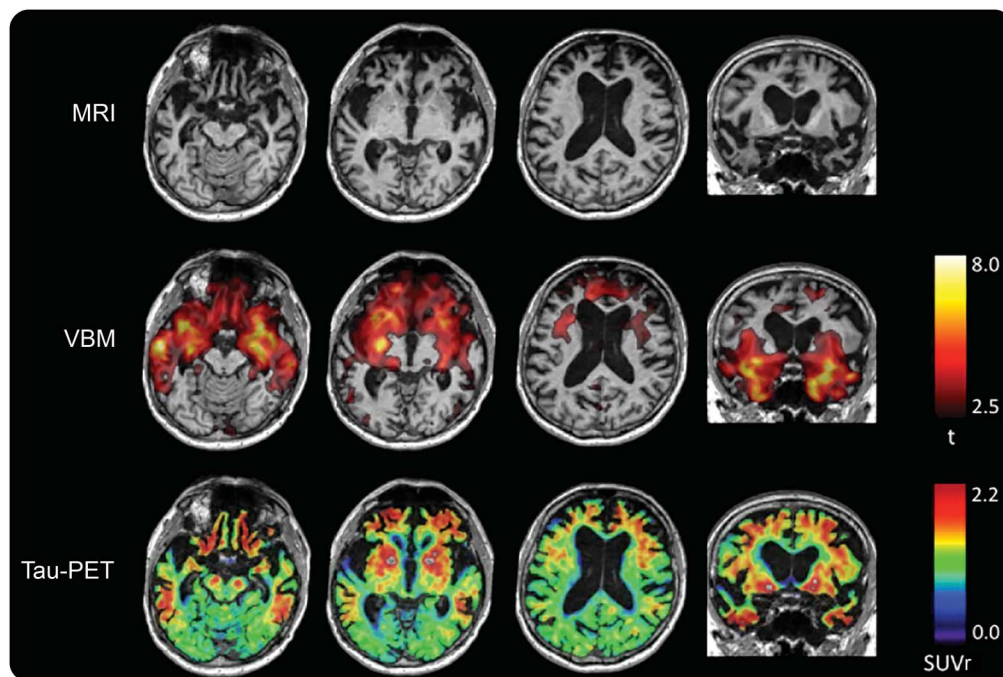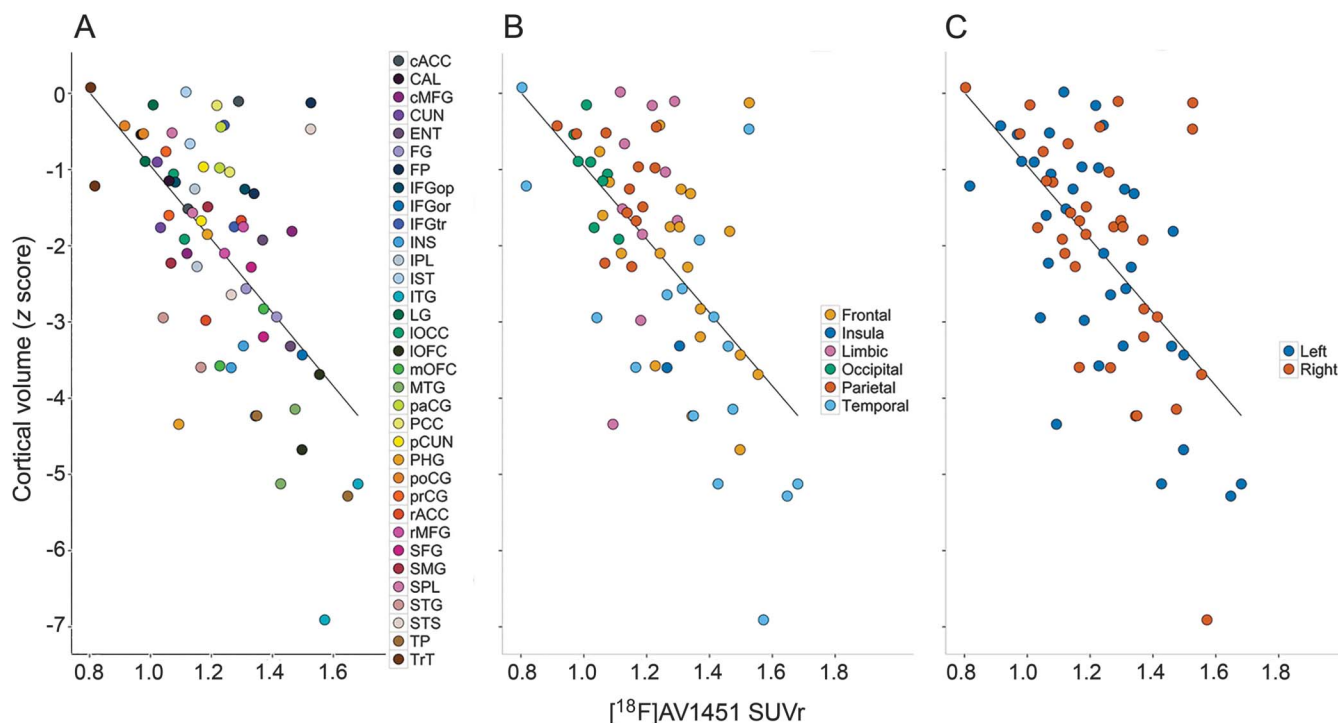
Structural T1 brain MRI (top row), gray matter volume loss (*p* < 0.01 uncorrected, middle row), and tau tracer binding (threshold 0–2.2) in the proband compared to normal controls. SUVr = standard uptake value ratio; VBM = voxel-based morphometry.

The substantia nigra was normal (figure 4C), and the locus coeruleus was moderately depigmented. The highest density of NFT, pretangles, and neuropil threads was observed in the middle frontal cortex, anterior cingulate gyrus, caudate nucleus, and amygdala; lesser density was seen in the lateral temporal cortex (figure 4, E and F). Sparse tau pathology was observed in the motor and occipital cortices. NFT morphology was similar to what was observed in AD. Neocortical laminar deposition, however, was more superficial, involving layer II with sparse to moderate NFTs observed in layer V pyramidal neurons. Pretangles and NFT were sparse in the putamen and globus pallidus. Ventral and anterior nucleus of the thalamus revealed mild NFT and thread pathology. Moderate NFTs were observed in the subthalamic nucleus, along with mild thread pathology. Mild neuronal loss and gliosis was observed in the substantia nigra, along with moderate NFT and thread pathology (figure 4D). Moderate NFT and thread pathology was also observed in the midbrain tectum, locus coeruleus, and pontine tegmentum. No tau pathology was observed in the cerebellum. Tau pathology was moderate in the parahippocampal region and sparse in the hippocampus (figure 4, H and I). Tufted-like tau-positive astrocytes (figure 4G) were seen in the putamen.

Sparse TDP-43–positive neuronal cytoplasmic inclusions and fine neurites were noticed in the CA1, dentate gyrus, and subiculum, together with extensive neuronal loss and gliosis, and consistent with neurodegenerative hippocampal sclerosis (figure 4, J–L). Bilobed, perivascular TDP-43 was commonly found in both the hippocampus and amygdala.[32] TDP-43 deposits were also seen in the basal forebrain, inferior olivary nucleus, basal ganglia, and some neocortical areas. Frequent diffuse and sparse Aβ plaques were observed in the neocortex. Neuritic plaques were seen in the CA1/subiculum, dentate gyrus, and CA4 of the hippocampus (intermediate AD neuropathologic changes). There were no amyloid angiopathy or α-synuclein–immunoreactive deposits.

Patient B.II.1. There was severe atrophy of the temporal pole, insula, amygdala, orbitofrontal cortex, and ventromedial striatum. Neuronal loss and gliosis were most severe in the subgenual cingulate and inferior temporal gyri. Astrogliosis was noted in the anterior orbital gyrus, middle and inferior frontal gyri, superior frontal sulcus, middle insula and entorhinal cortex, amygdala, thalamus, substantia nigra, dorsal and median raphe, and periaqueductal gray. Mild NFT pathology was seen in the entorhinal cortex, CA1/subiculum, and median raphe. Pretangles were abundant in the frontal pole, anterior orbital gyrus, middle and inferior frontal gyrus, anterior cingulate

Correlations between [¹⁸F]AV1451 standardized uptake value ratio (SUVr) and regional brain volume in the proband (A). Anatomic regions are grouped by cerebral lobes (B) and by side of cerebral hemisphere (C). cACC = caudal anterior cingulate cortex; CAL = calcarine cortex; cMFG = caudal middle frontal gyrus; CUN = cuneus; ENT = entorhinal cortex; FG = fusiform gyrus; FP = frontal pole; IFGop = inferior frontal gyrus pars opercularis; IFGor = inferior frontal gyrus pars oralis; IFGtr = inferior frontal gyrus pars triangularis; INS = insula; IPL = inferior parietal lobule; IST = isthmus of the cingulate gyrus; ITG = inferior temporal gyrus; LG = lingular gyrus; lOCC = lateral occipital cortex; lOFC = lateral orbitofrontal cortex; mOFC = medial orbitofrontal cortex; MTG = middle temporal gyrus; paCG = paracentral gyri; PCC = posterior cingulate cortex; pCUN = precuneus; PHG = parahippocampal gyrus; poCG = postcentral gyrus; prCG = precentral gyrus; rACC = rostral anterior cingulate cortex; rMFG = rostral middle frontal gyrus; SFG = superior frontal gyrus; SMG = supramarginal gyrus; SPL = superior parietal lobule; STG = superior temporal gyrus; STS = superior temporal sulcus; TP = temporal pole; TrT = transverse temporal gyrus.

cortex ventral striatum, subgenual cingulate cortex, temporal cortex, amygdala, middle insula, CA1/subiculum, entorhinal cortex, periaqueductal gray, median raphe, facial nucleus, thalamus, and subthalamic nucleus (figure 5, A–D). Sparse pretangles were noted in the precentral gyrus, angular gyrus, posterior cingulate cortex, putamen, globus pallidus, CA3-4, and substantia nigra. Abundant thread pathology was found in cortical layers II, V, and VI of the most affected areas, together with moderate oligodendroglial inclusions in the corresponding white matter. All tau-immunoreactive inclusions were stained with both 3R and 4R tau antibodies (figure 5, E and F).

Lewy bodies and/or neurites were seen in the cingulate cortex, amygdala, dorsal motor nucleus of the vagus nerve, entorhinal cortex, substantia nigra, raphe nuclei, and hypoglossal nucleus. No Aβ or pathologic TDP-43 immunostaining was observed.

DISCUSSION We report clinical, neuropsychological, structural, and tau protein molecular imaging data on a symptomatic carrier of the V337M *MAPT* mutation. The main findings are the following: (1)

the anatomic distribution of tau pathology as assessed by postmortem neuropathologic study of the brains of the proband's mother and of a nonrelated carrier of the *MAPT* V337M mutation strikingly matches the topography and degree of [¹⁸F]AV1451 tracer retention in the proband; (2) a significant correlation was observed between the degree of regional MRI brain atrophy and the extent of [¹⁸F]AV1451 binding in the proband; and (3) a strong association between the proband's clinical presentation and the extent of regional brain atrophy and tau accumulation as assessed by structural brain MRI and [¹⁸F]AV1451 PET was observed.

The highest extent of tau tracer binding in the proband's frontal pole, medial orbitofrontal cortex, inferior temporal lobe, insular cortex, anterior cingulate, dorsolateral prefrontal cortex, and lateral temporal cortex strongly recapitulates the distribution of tau pathology in the proband's mother and in the unrelated V337M mutation carrier. Only a mild extent of NFT pathology was noted in the proband's mother's and in the unrelated V337M carrier's hippocampus, which recapitulates the sparing of tau tracer binding

**Figure 4** Neuropathologic findings in the proband's mother
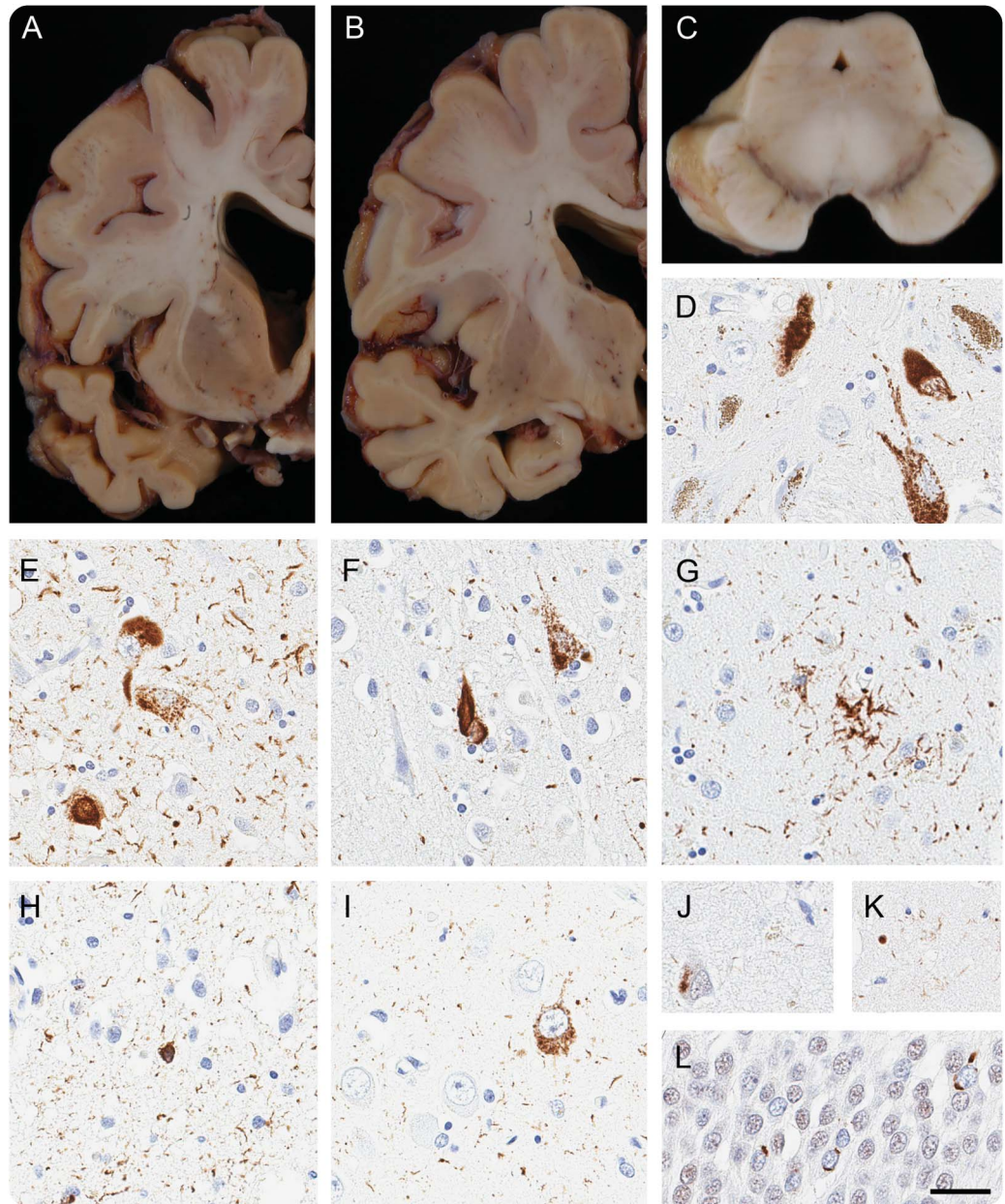
Macroscopic examination of the proband's mother's brain shows significant frontal atrophy (A and B), temporal atrophy (A), and hippocampal atrophy (B). There was no evident macroscopic depigmentation of the substantia nigra (C). Representative photomicrographs immunohistochemically stained for phosphorylated tau (CP13) (D–I) and TDP-43 pathology (J–L). Moderate pretangles and neuropil threads were observed in the substantia nigra (D). Pretangles and neuropil threads were frequently observed in the frontal cortex (E), were of moderate severity in the temporal cortex (F), and were sparsely observed in the entorhinal cortex (H). Tuft-like tau-positive astrocytes were found almost exclusively in the putamen (G). Hippocampal neuronal loss was disproportionate to the burden of tau-positive structures (I). TDP-43–positive neuronal cytoplasmic inclusions (J) and fine neurites consistent with hippocampal sclerosis were found throughout the CA1 and subiculum of the hippocampus (K). Perinuclear TDP-43–positive neuronal cytoplasmic inclusions in the dentate fascia were found in moderate density (L). Scale bar for D–L = 30 μm. TDP-43 = TAR DNA binding protein–43 kDa.

in the same region of the proband. Intermediate levels of tracer uptake in the proband's entorhinal cortex are consistent with the either moderate (proband's mother) or mild (unrelated carrier) extent of postmortem tau pathology. Elevated tau tracer binding was found in the proband's ventral striatum, the same region where severe tau pathology was observed in the unrelated V337M carrier. However, correlations between [18F]AV1451 and tau pathology in subcortical nuclei should be cautiously interpreted because elevated [18F]AV1451 binding in these regions is seen in cognitively normal older adults, increases with older age, and is thought to represent off-target ligand binding unrelated to tau.[14,17,18] The neuropathologic

Figure 5   Neuropathologic findings in an unrelated V337M *MAPT* mutation carrier
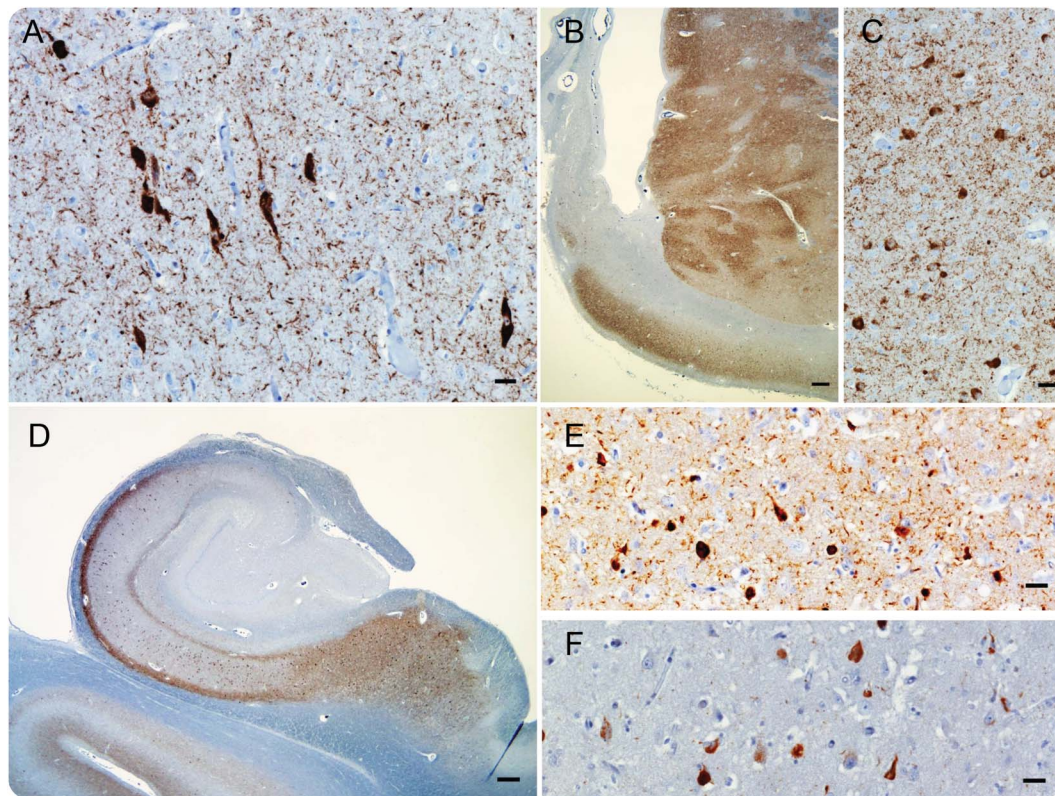
Neuropathologic assessment of patient B.II.I. Abundant tau-immunoreactive neurons and neuropil threads in layer V of the anterior cingulate gyrus (A). Severe tau deposition in neurons and neuropil of the ventral striatum (B and C). Tau-immunoreactive neurons and neuropil threads in the hippocampus (mild) and subiculum (moderate) (D). Tau-immunoreactive neurons and neuropil threads in the subgenual cingulate gyrus are immunoreactive against 3-repeat tau (E) and 4-repeat tau (F). Immunohistochemistry: CP13 (A–D), RD3 (E), and RD4 (F). Scale bars: 25 μm (A, C, E, and F) and 500 μm (B and D).

findings from our study are consistent with the findings described in the original report on the V337M *MAPT* mutation pathology, which also confirmed the presence of PHF with electron microscopy.[11] All tau-immunoreactive inclusions in the unrelated V337M carrier were stained with both 3R and 4R tau antibodies, although we were not equipped to perform electron microscopy to confirm the PHF of tau. These findings suggest the high affinity of [18F]AV1451 for PHF tau inclusions containing all 6 tau isoforms, as found in AD and in a subset of *MAPT* mutations, including V337M.[14,19] It is unlikely that [18F]AV1451 retention reflects binding to concurrent AD pathology in the proband, given the atypical distribution (frontotemporal, with notable sparing of posterior cortical areas), the proband's normal CSF Aβ$_{42}$ levels, and the lower SUVr values compared to the AD range.[25] VBM assessment of the proband's brain atrophy showed predominantly bilateral anterior and inferolateral temporal, orbitofrontal, and insular involvement. Medial temporal lobes regions were also atrophic although better preserved. Posterior regions of the brain were less affected. These findings strongly correlate with the regional distribution of the proband's tau tracer uptake profile and with his clinical presentation and support interdependence among tau pathology distribution, clinical phenotype, and neurodegeneration.

Our data parallel a recent report highlighting the correlation between [18F]AV1451 binding and the extent and topographical distribution of tau pathology in carriers of the R406W *MAPT* mutation, also known to result in accumulation of AD-like PHF filaments composed of all 6 isoforms of tau.[19] [18F]AV1451 PET assessment of a 56-year-old man with bvFTD associated with the P301L *MAPT* mutation has shown frontotemporal ligand uptake closely resembling the anatomic distribution of tau pathology in *MAPT*-related familial FTD.[33,34] Our group has described a patient with posterior cortical atrophy, the parieto-occipital variant of AD, who underwent 18FDG= fluorodeoxyglucose PET, Aβ PET scan ([11C] Pittsburgh compound B), and [18F]AV1451 tau PET. The predominant pattern of [18F]AV1451 retention in the posterior cortical regions overlapped with the areas of diminished hypometabolism. In contrast, [11C]Pittsburgh compound B binding was diffusely distributed among several

cortical areas with no correlation with regional metabolism.[16] Finally, we showed the association between pattern and extent of tau pathology and clinical symptoms secondary to selective neurodegeneration in a larger cohort of patients with AD with heterogeneous clinical and anatomical presentation.[25]

Our study has limitations. First, [18F]AV1451 PET and pathologic findings were not obtained from the same individual. Second, we did not correct PET data for partial volume signal loss due to atrophy, which was profound in frontotemporal regions, leading to likely underestimation of true tracer retention. However, atrophy would only bias against our detecting meaningful [18F]AV1451 signal and negative correlations with neurodegeneration in the proband. We were unable to assess the degree of basal ganglia binding in the proband compared to controls because we have not studied an age-matched control group with [18F]AV1451 PET. The marked correspondence between regions of [18F]AV1451 retention in the proband and tau pathology in his mother suggests that [18F]AV1451 labeled tau pathology in the proband. Further studies are needed to fully characterize the potential of [18F]AV1451 and other emerging tau ligands to detect pathology across the spectrum of mutations and clinical stages of *MAPT*-associated FTLD.

AUTHOR CONTRIBUTIONS

ACKNOWLEDGMENT

STUDY FUNDING

DISCLOSURE

REFERENCES

1. Ratnavalli E, Brayne C, Dawson K, Hodges JR. The prevalence of frontotemporal dementia. Neurology 2002;58: 1615–1621.
2. Onyike CU, Diehl-Schmid J. The epidemiology of frontotemporal dementia. Int Rev Psychiatry 2013;25:130–137.

3. Rascovsky K, Hodges JR, Knopman D, et al. Sensitivity of revised diagnostic criteria for the behavioural variant of frontotemporal dementia. Brain 2011;134:2456–2477.

4. Gorno-Tempini ML, Hillis AE, Weintraub S, et al. Classification of primary progressive aphasia and its variants. Neurology 2011;76:1006–1014.

5. Hutton M, Lendon CL, Rizzu P, et al. Association of missense and 5'-splice-site mutations in tau with the inherited dementia FTDP-17. Nature 1998;393:702–705.

6. Clark LN, Poorkaj P, Wszolek Z, et al. Pathogenic implications of mutations in the tau gene in pallido-ponto-nigral degeneration and related neurodegenerative disorders linked to chromosome 17. Proc Natl Acad Sci USA 1998;95: 13103–13107.

7. Poorkaj P, Bird TD, Wijsman E, et al. Tau is a candidate gene for chromosome 17 frontotemporal dementia. Ann Neurol 1998;43:815–825.

8. Spillantini MG, Murrell JR, Goedert M, Farlow MR, Klug A, Ghetti B. Mutation in the tau gene in familial multiple system tauopathy with presenile dementia. Proc Natl Acad Sci USA 1998;95:7737–7741.

9. van Swieten J, Spillantini MG. Hereditary frontotemporal dementia caused by tau gene mutations. Brain Pathol 2007;17:63–73.

10. Bird TD, Wijsman EM, Nochlin D, et al. Chromosome 17 and hereditary dementia: linkage studies in three non-Alzheimer families and kindreds with late-onset FAD. Neurology 1997;48:949–954.

11. Sumi SM, Bird TD, Nochlin D, Raskind MA. Familial presenile dementia with psychosis associated with cortical neurofibrillary tangles and degeneration of the amygdala. Neurology 1992;42:120–127.

12. Spillantini MG, Crowther RA, Goedert M. Comparison of the neurofibrillary pathology in Alzheimer's disease and familial presenile dementia with tangles. Acta Neuropathol 1996;92:42–48.

13. Xia CF, Arteaga J, Chen G, et al. [(18)F]T807, a novel tau positron emission tomography imaging agent for Alzheimer's disease. Alzheimers Dement 2013;9:666–676.

14. Marquie M, Normandin MD, Vanderburg CR, et al. Validating novel tau positron emission tomography tracer [F-18]-AV-1451 (T807) on postmortem brain tissue. Ann Neurol 2015;78:787–800.

15. Chien DT, Bahri S, Szardenings AK, et al. Early clinical PET imaging results with the novel PHF-tau radioligand [F-18]-T807. J Alzheimers Dis 2013;34:457–468.

16. Ossenkoppele R, Schonhaut DR, Baker SL, et al. Tau, amyloid, and hypometabolism in a patient with posterior cortical atrophy. Ann Neurol 2015;77:338–342.

17. Johnson KA, Schultz A, Betensky RA, et al. Tau positron emission tomographic imaging in aging and early Alzheimer disease. Ann Neurol 2016;79:110–119.

18. Lowe VJ, Curran G, Fang P, et al. An autoradiographic evaluation of AV-1451 tau PET in dementia. Acta Neuropathol Commun 2016;4:58.

19. Smith R, Puschmann A, Scholl M, et al. 18F-AV-1451 tau PET imaging correlates strongly with tau neuropathology in *MAPT* mutation carriers. Brain 2016;139:2372–2379.

20. Josephs KA, Whitwell JL, Tacik P, et al. [¹⁸F]AV-1451 tau-PET uptake does correlate with quantitatively measured 4R-tau burden in autopsy-confirmed corticobasal degeneration. Acta Neuropathol 2016;132:931–933.

21. Yokoyama JS, Sturm VE, Bonham LW, et al. Variation in longevity gene KLOTHO is associated with greater cortical volumes. Ann Clin Transl Neurol 2015;2:215–230.

22. Lehmann M, Ghosh PM, Madison C, et al. Diverging patterns of amyloid deposition and hypometabolism in clinical variants of probable Alzheimer's disease. Brain 2013;136:844–858.

23. Fischl B, van der Kouwe A, Destrieux C, et al. Automatically parcellating the human cerebral cortex. Cereb Cortex 2004;14:11–22.

24. Fischl B, Dale AM. Measuring the thickness of the human cerebral cortex from magnetic resonance images. Proc Natl Acad Sci USA 2000;97:11050–11055.

25. Ossenkoppele R, Schonhaut DR, Scholl M, et al. Tau PET patterns mirror clinical and neuroanatomical variability in Alzheimer's disease. Brain 2016;139:1551–1567.

26. Baker SL, Lockhart SN, Price JC, et al. Reference tissue-based kinetic evaluation of 18F-AV-1451 in aging and dementia. J Nucl Med. Epub 2016 Sep 1.

27. Shaw LM, Vanderstichele H, Knapik-Czajka M, et al. Cerebrospinal fluid biomarker signature in Alzheimer's disease neuroimaging initiative subjects. Ann Neurol 2009;65:403–413.

28. Mirra SS, Heyman A, McKeel D, et al. The Consortium to Establish a Registry for Alzheimer's Disease (CERAD), part II: standardization of the neuropathologic assessment of Alzheimer's disease. Neurology 1991;41:479–486.

29. Hyman BT, Phelps CH, Beach TG, et al. National Institute on Aging-Alzheimer's Association guidelines for the neuropathologic assessment of Alzheimer's disease. Alzheimers Dement 2012;8:1–13.

30. Murray ME, Cannon A, Graff-Radford NR, et al. Differential clinicopathologic and genetic features of late-onset amnestic dementias. Acta Neuropathol 2014;128:411–421.

31. Mackenzie IR, Neumann M, Baborie A, et al. A harmonized classification system for FTLD-TDP pathology. Acta Neuropathol 2011;122:111–113.

32. Lin WL, Castanedes-Casey M, Dickson DW. Transactivation response DNA-binding protein 43 microvasculopathy in frontotemporal degeneration and familial Lewy body disease. J Neuropathol Exp Neurol 2009;68:1167–1176.

33. Spina S, Farlow MR, Unverzagt FW, et al. The tauopathy associated with mutation +3 in intron 10 of tau: characterization of the MSTD family. Brain 2008;131:72–89.

34. Ghetti B, Oblak AL, Boeve BF, Johnson KA, Dickerson BC, Goedert M. Frontotemporal dementia caused by MAPT mutations: a chameleon for neuropathology and neuroimaging. Neuropathol Appl Neurobiol 2015;41:24–46.